Data Repository Item

Micro-scale heterogeneity of Fe isotopes in >3.71 Ga banded iron formation from the Isua Greenstone Belt, southwest Greenland.

M. J. Whitehouse and C. M. Fedo

SAMPLE DESCRIPTIONS

Samples IS-02-05, IS-02-06, and IS-02-08 represent variants of typical "quartz - magnetite" BIF from the northeastern part of the IGB (Fig. DR1) (Dymek and Klein, 1988). The latter two primarily consist of mm-scale magnetite and quartz alternations (Fig. DR2). Minor amounts of finely disseminated green amphibole occur within quartz bands in sample IS-02-06. We interpret the quartz as coarsely recrystallized depositional chert. In contrast, sample IS-02-05 has less quartz, consisting of alternating mm-scale bands of oriented beige amphibole needles + quartz and magnetite (Fig. DR2), the amphibole most likely derived from ferroan dolomite or minnesotaite (Klein, 2005). All samples have experienced ductile deformation and some contain a prominent mineral stretching lineation parallel to the plunge direction of the major synform that comprises this tectonic domain (Myers, 2001).

Two samples of secondary pyrite were selected from rocks in the same tectonic domain to investigate the Fe isotope characteristics of clearly post-depositional iron-bearing phases in highly contrasting host lithologies. Sample 248474 is a BIF consisting of alternating bands of magnetite and quartz which contains secondary pyrite occurring as irregular accumulations within the cores of small-scale fold hinges and as veinlets discordant to the main layering. Previous SIMS analysis of this pyrite (Whitehouse et al., 2005) has revealed a Pb isotopic composition consistent with its formation in the Early Archean and a positive mass independent fractionated sulfur composition ($\Delta^{33}S$ = +3.3 ‰). The second sample, 462622, comes from a prominent pebble-to-cobble polymictic conglomerate of volcaniclastic origin (Fedo, 2000) that contains secondary pyrite as euhedral and subhedral cubes.

Sample 409041 was collected from a kilometer-scale enclave of mafic-ultramafic and supracrustal rocks that occurs in 3.81 Ga tonalitic gneisses (Nutman et al., 1999), approximately 10 km southwest of the southernmost point of the IGB (25 km SW of sample 462622). This and similar enclaves in the early Archean gneisses possibly represent dismembered analogues of the IGB itself (Fedo et al., 2006). The sample consists of alternating < 5 mm thick bands of pyroxene + amphibole + magnetite and quartz.

ANALYTICAL METHODS

1. Sample preparation

Representative chips of the four rock samples and separated pyrites were cast in epoxy together with characterized reference standards (Table DR1), magnetite "LP-204" (Valley and Graham, 1999), pyrite "Balmat" (Crowe and Vaughan, 1996). Individual crystals of magnetite were selected from each sample based on examination by reflected light microscopy on the polished epoxy mount. The total area available for grain selection in each sample was approximately 10-25 mm^2.

2. Secondary ion mass spectrometry

High spatial resolution Fe isotope compositions were determined using a Cameca IMS1270 ion microprobe at the Swedish Museum of Natural History (NordSIMS facility). Instrument operating parameters are described below.

Primary ion beam: An O_2^- primary beam was used with incident energy of 23 kV. Projection of the primary column mass aperture onto the surface of the sample produced elliptical, flat-bottomed sputtering craters with long axes of ca. 25 μm (200 μm aperture) or 18 μm (150 μm aperture) and corresponding ion beam currents of ca. 10 nA or 6 nA.

Secondary ion beam: Positive secondary ions were extracted at 10 kV with a field magnification of ca. 50 x at the 3000 μm field aperture. This gives an effective field of view on the sample of

60 x 60 μm which ensures that there is no clipping of signal by the field aperture. An entrance slit width of 60 μm was used together with the largest contrast aperture (400 μm) to define the shape of the ion beam admitted to the mass spectrometer. An energy window of 60 eV was used throughout this study and the secondary ion optics were operated in the "circular" mode in order to accommodate the ion beam in the restricted height of the multicollector exit slits (see discussion in Whitehouse, 2004).

Detector configuration: The detector configuration was selected to accommodate simultaneous Faraday cup measurement of ^{54}Fe, ^{56}Fe and ^{57}Fe in both sulfides and magnetite. Since the latter commonly contain small amounts of Cr, it is necessary to monitor and correct for a possible ^{54}Cr isobaric interference on ^{54}Fe using an additional low mass detector to measure ^{53}Cr; the low ^{53}Cr signal required an electron multiplier. The actual detector configuration used is shown in Fig. DR3a and comprised a low mass EM (detector designation L2) to measure ^{53}Cr, an FC (L1) to measure ^{54}Fe, an EM (C) positioned on the instrument axis and connected to the secondary ion imaging system to facilitate coarse centering of the beam in the field aperture, an FC (H1) to measure ^{56}Fe and an FC (H'2) to measure ^{57}Fe. All Faraday detectors were connected to amplifiers with 10^{11} Ω input resistors, housed in an evacuated chamber that was heated slightly above ambient in order to maintain stable levels of background. The EM detector used to measure ^{53}Cr was connected to a pulse counting system with a noise level < 2 counts per minute and an electronically gated dead time of 60 ns. The EM gain relative to the FC's was adjusted to be within ca. ± 5% of unity. At the relatively low levels of Cr encountered in this study, both gain and dead time corrections on ^{54}Fe were very small and did not result in significant bias on the Fe-isotope ratio determination.

Interferences and mass resolution: Aside from the possible isobaric interference of ^{54}Cr on ^{54}Fe, the only other significant direct interference is that of ^{56}Fe^{1}H on ^{57}Fe. In order to separate these species, a high mass resolution requirement of ca. 7500 (M/ΔM) is required. This is shown in Figure DR3b as a superimposed high mass resolution peak in which the ^{57}Fe and ^{56}Fe^{1}H are clearly resolved. The level of hydride formation is about 0.2 ‰. On the IMS1270, this can be achieved using an exit slit width of 150 μm (the multicollector exit slits are user selectable at fixed settings common to all channels of 150 μm, 250 μm and 500 μm); however, since ^{57}Fe is

the lowest signal and its measurement is not of great importance in SIMS (cf. ICP measurements where it is essential to monitor both ^{56}Fe and ^{57}Fe in order to assess the significance of $^{40}Ar^{16}O^{+}$ (from the plasma) interference on $^{56}Fe^{+}$ and $^{40}Ar^{16}O^{1}H^{+}$ on $^{57}Fe^{+}$), the present method utilized a 250 μm exit slit (in some later homogeneity test sessions and for pyrite 500 μm) in order to maximize the peak flat on the ^{54}Fe and ^{56}Fe detectors (Fig. DR3b). The ^{57}Fe detector was positioned on the narrow ^{57}Fe only peak flat on the low mass side of the combined peak. Minor hydride contributions are expected also on the ^{53}Cr peak (from $^{52}Cr^{1}H$) and on the ^{54}Fe peak ($^{53}Cr^{1}H$) but the low level of Cr encountered in magnetite (absent entirely in pyrite) during this study means that these minor contributions can be ignored. In order to minimize further contributions, the liquid N_2 cold trap on the sample chamber was utilized, ensuring that sample chamber pressure was typically around or better than 10^{-8} mbar. Correlation plots of $\delta^{57}Fe$ against $\delta^{56}Fe$ for all data obtained during this study (Figs. DR4 and DR5a) yield the expected slope of the mass dependent fractionation line (ca. 1.5), showing that hydride contributions to the ^{57}Fe signal resulting from a tail of the hydride peak was negligible.

Mn presents a potential hydride interference of $^{55}Mn^{1}H$ on ^{56}Fe. Since Mn is mono-isotopic, there are no options for directly monitoring the level of hydride formation during an analysis. As noted in the section below on matrix effects, Mn was absent from our analysed Isua magnetites but is present at a low level (2.7 wt. %) in the LP-204 reference magnetite (Sitzman et al., 2000). Separation of $^{55}Mn^{1}H$ from ^{56}Fe requires a mass resolution of ca. 5000 ($M/\Delta M$) which is achieved using the 250 μm exit slit applied during analysis of the Isua magnetites. To further assess the possible magnitude of the Mn hydride during later analyses with a 500 μm exit slit, several analyses were made of LP-204 at a mass resolution of 5000 using a monocollection routine to measure ^{55}Mn, ^{56}Mn and $^{55}Mn^{1}H$. The ratio $^{55}Mn^{1}H/^{55}Mn$ was ca. 3×10^{-4}, indicating a ca. 0.3 ‰ level of hydride formation consistent with that noted above for Fe hydride. The corresponding $^{55}Mn^{1}H/^{56}Fe$ ratio was ca. 4×10^{-5} implying a potential perturbation of Fe isotope ratios involving 56Fe of only ca. 0.04 ‰, well within the analytical uncertainty of our SIMS measurements.

Other minor interferences that might be encountered in magnetite are from minor substitutions of Al (hercynite component) and Mg. Al and Mg will generate molecular species $^{26}Mg^{27}Al^{+}$ (visible

to the high mass side on ^{53}Cr in Figure DR3b) at nominal mass 53 and $^{27}Al_2^+$ at nominal mass 54. Even operating at the lowest mass resolution of the instrument in multicollector mode (500 μm exit slit) however, these species do not overlap with the ^{53}Cr and ^{54}Fe peaks of interest and can therefore be ignored.

Analysis protocol: Initial coarse centering of the beam in the field aperture was performed for the centre of each sample mount using the secondary ion imaging system (connected to the EM channel L2) to view a 250 x 250 μm raster area of either ^{197}Au (from the 30 nm Au coating) or ^{56}Fe from a mineral (a sufficient Fe signal for this purpose is readily obtained after a few seconds of sputtering and enables centering to be performed before the EM detector saturation count rate is reached). The position of the image was centered using the final deflectors of the primary column (D4_x and D4_y). After this step, the D4 deflectors were kept constant and changes in beam centering resulting from small sample height variations were accommodated using the transfer deflectors (DT1_x and DT1_y) acting on the secondary beam.

Analyses were performed in chain sequences in order to keep conditions as reproducible as possible. Within the automated sequence, each individual analysis consisted of a 120 second pre-sputter over a raster area of 25 x 25 μm, during which time the secondary beam was blanked so that the FC detector backgrounds could be measured. At the end of the pre-sputter period, the raster was removed and centering of the beam in the field aperture was performed by scanning the transfer deflectors. This was followed by a mass scan to correct for any long term drift of the secondary magnet field and a scan of the sample high-voltage in order to reproduce the position of the beam in the energy slit and thus minimize any possible sample charging effects (generally these were small, varying by less than ±1 eV within the analytical session, because the target materials were conductors). Finally, data were acquired for either 180 or 240 seconds (this parameter depended on count rate determined prior to starting the automated sequence) using 10 second integrations.

Matrix effects: Instrumental mass fractionation may result from differences in matrix composition and structure which affects sputtering characteristics for different elements, particularly those of interest for light stable isotopes. In order to assess the possibility that our data might be affected

by such matrix effects, we undertook post-analytical quantitative SEM-EDS measurements of the analysed magnetite grains adjacent to the point of analysis, as well as analyses of the reference LP-204 magnetite. In the sample magnetite grains, the only trace element detected was Al, which was present at 0.9 wt.% in IS-02-05 grain #2, and at 0.5 wt. % in IS-02-05 grain # 1 and IS-02-08 grain #7, but below detection limit in all other grains. There is no correlation evident between these contents and the $\delta^{56}Fe$ values (see Fig. DR7), suggesting that they are below a level that will induce significant matrix effects at the precision level of these measurements. Several SEM-EDS analyses of the LP-204 reference magnetite revealed an average Al content of ca. 1% and an average Mn content of ca. 3%. With the exception of Mg which is below the detection limit of the system, these values are consistent with the trace element composition of this magnetite of $Mg_{0.056}Al_{0.070}Mn_{0.113}Fe^{2+}_{0.831}Fe^{3+}_{1.930}O_4$ reported by Sitzman et al. (2000), who further showed that Al and Mn are hosted in homogeneously distributed nm-sized platelets of Al – Mn (± Fe) spinel (possibly hercynite-galaxite mixtures). Exsolution of trace Al and Mn into the nano-inclusions implies that the bulk of the Fe analysed from LP-204 is sputtered from a near-ideal Fe_3O_4 magnetite matrix similar in composition to our unknown magnetites and for this reason we would not expect any significant matrix effects to arise from using Mn-bearing LP-204 to standardize Mn-absent magnetite unknowns. In the event that small matrix effects do occur, the homogeneity of LP-204 composition means that these would result in a systematic bias to all analyses but still would be unable to account for the heterogeneity observed in our samples.

Data reduction: Unknown analyses were interspersed with analyses of the reference magnetite or pyrite (Fig. DR6). For each session, the ^{53}Cr interference on ^{54}Fe was first stripped assuming a $^{54}Cr/^{53}Cr$ ratio of 0.24843 and a relative detector gain of 0.95 with an arbitrarily assigned and propagated error of ± 0.05. Instrumental mass bias and possible minor hydride contributions to this ratio were ignored and are considered to be covered by the assigned error. For the LP-204 reference magnetite, this correction was a very consistent ca. 0.040 ± 0.001 ‰ on the $^{56}Fe/^{54}Fe$ ratio; for the unknown magnetites the correction ranged from 0.01 ‰ to 0.06 ‰. Data were then assessed for possible within session drift by plotting the standard data in order of acquisition. Drift was observed in two of the magnetite sessions which showed a monotonic increase in both $^{56}Fe/^{54}Fe$ (0.07 ‰/run and 0.06 ‰/run) and $^{57}Fe/^{54}Fe$ (0.11 ‰/run and 0.09 ‰/run). The cause of this drift is unclear but might be related to changes in primary beam density due to erosion of

the projected mass aperture or detector gain drift. Because the drift occurs along the mass fractionation line (the drift in $^{56}Fe/^{54}Fe$ is ca. 1.5 x that in $^{57}Fe/^{54}Fe$), detector gain drift is considered unlikely and, if the primary cause, would have to be in the common detector measuring ^{54}Fe.

Following correction for Cr interference and possible session drift, reference analyses were averaged to yield an external standard deviation. The assumed Fe-isotope composition of the standard relative to IRMM (see standard characterization section below) was used to derive the composition of the unknown and its internal error (typically < ±0.1 ‰, 1σ) was propagated together with the generally larger external error (typically ca. ±0.2 ‰, 1σ) to yield an overall uncertainty on each determination.

Systematic errors: During the course of this study unexpectedly large variations in Fe isotope composition were noted from a number of standard and unknown analyses which highlight potential pitfalls related to beam placement. One of these is illustrated by analysis #5 of sample IS-02-08 which yielded the highest apparent $\delta^{56}Fe$ value obtained from this sample (Table DR2) and with a substantial higher internal error (±0.4 ‰ (1σ) compared to < ±0.1 ‰ for all other analyses). Post-analytical examination of the analysis site revealed that the primary ion beam partly overlapped onto an adjacent quartz grain (Fig. DR7c, panel D). Since emission from the sample spot is unlikely to be entirely homogenous with respect to isotopic fractionation, the entire analysis from such a partially occluded spot will be fractionated to a different degree from a crater that is completely contained in the mineral species of interest.

A second example of systematic error is illustrated by analysis LP-D@6 obtained during the magnetite reference homogeneity tests. This analysis yielded high $\delta^{56}Fe$ and $\delta^{57}Fe$ values that represent marked outliers in the group of reference analyses (Table DR3). Post-analytical examination of the sample revealed that the ion beam sampled a prominent crack traversing the magnetite grain. As a result of these observations, all sample locations were examined by reflected light microscopy in order to screen out analyses affected by such systematic errors.

Standard characterization and homogeneity tests: Two magnetites were selected for possible use as reference materials. LP-204 is a commonly used oxygen isotope standard (Valley and Graham, 1991) and was kindly provided by J. Valley. LS68 is magnetite from the Laco Sur, El Laco volcano in Chile (lat. S23°48', W67°30'; Nyström and Henríquez, 1994) kindly provided by J.-O. Nyström. For pyrite standardization, the commonly used sulphur isotope standard Balmat (Crowe and Vaughan, 1996) was used. Two crystals of each of these potential standards were analysed by solution MC-ICP- MS at the Institute for Mineralogy, University of Hannover using previously described techniques (Schoenberg and von Blanckenburg, 2005). In addition to the Balmat pyrite, two crystals of pyrite from Isua sample 248474 were also analysed. Individual MC-ICP-MS analyses are presented in Table DR1.

The LP-204 magnetite crystal that was used during these analyses (designated LP-D) was mounted in epoxy together with four other crystals (designated LP-A, LP-B, LP-C and LP-E) as well as four crystals of the LS68 magnetite (designated EL-1, EL-2, EL-3 and EL-4). These magnetites (excepting LP-C and EL-4 which polished poorly) were analysed during a single analytical session in which LP-D was used as the "reference" material assuming the MC-ICP-MS value of $\delta^{56}Fe$ = -0.375 ‰. Time interleaved data are reported in Table DR3 and shown in Figure DR5b with the averages obtained from each crystal shown as uncertainty bars in Figure 1 (main manuscript). These data reveal some heterogeneity in LP-204 which may introduce a systematic ca. < 0.25 ‰ error in unknown analyses depending on which grain is used for characterization. Within the context of this study, such an uncertainty is acceptable and these data indicate that LP-204 is an appropriate reference material for in situ SIMS studies. In contrast, the magnetite crystals from LS68, while internally relatively homogenous, show a wide inter-grain variation in $\delta^{56}Fe$ of >0.8 ‰ which renders them inappropriate as a SIMS reference material.

Similar homogeneity tests were carried out on three grains of the Balmat sulfide A, B and C which were mounted together in an epoxy mount with data reported in Table DR2. Data were obtained in two analytical sessions, the first of which had a relatively high external precision on $\delta^{56}Fe$ based on the grain A analyses of ± 0.23 ‰ (1σ) due to an instrument problem limiting transmission at the time. Relative to grain A with an assumed $\delta^{56}Fe$ = -0.399 ‰ from MC-ICP-

MS measurements, four analyses of grain C yield a weighted average $\delta^{56}Fe$ of -0.18 ± 0.23 (95% conf.). The second session in contrast had unrealistically low external precision of ± 0.04 ‰ (1σ), similar to the internal precision. A mean of five analyses of grains A and C with an assigned external error of ±0.16 ‰ (1σ; similar to that observed during longer analytical sessions) yielded $\delta^{56}Fe$ = -0.39 ± 0.18 ‰ (95% conf.). These data suggest that Balmat is sufficiently homogeneous to use as a SIMS Fe isotope standard. In addition to the homogeneity tests, a measure of the suitability of Balmat as a standard is given by the excellent agreement obtained between SIMS analyses of the 248474 pyrite (weighted average $\delta^{56}Fe$ = 0.95 ± 0.1 ‰ (95% conf., MSWD = 0.44, n = 8) and the MC-ICP-MS determination of $\delta^{56}Fe$ = 0.94 ± 0.25 ‰ based on the weighted average of two separate analyses.

POST ANALYTICAL SPOT DOCUMENTATION

The position of each analytical site was documented using reflected light microscopy at 200x magnification following removal of the gold coating. These images are shown in Fig. DR7.

References

Crowe, D.E., and Vaughan, R.G., 1996, Characterisation and use of isotopically homogeneous standards for in situ laser microprobe analysis of $^{34}S/^{32}S$ ratios: American Mineralogist, v. 81, p. 187-193.

Nyström, J.O., and Henríquez, F., 1994, Magmatic features of iron ores of the Kiruna type in Chile and Sweden: Ore textures and magnetite geochemistry: Economic Geology, v. 89, p. 820-839.

Schoenberg, R., and von Blanckenburg, F., 2005, An assessment of the accuracy of stable Fe isotope ratio measurements on samples with organic and inorganic matrices by high-resolution multicollector ICP-MS: International Journal of Mass Spectrometry, v. 242, p. 257-272.

Sitzman, S.D., Banfield, J.F. and Valley, J.W., 2000, Microstructural characterization of metamorphic magnetite crystals with implications for oxygen isotope distribution: American Mineralogist, v. 85, p. 14-21.

Valley, J.W.. and Graham, C.M., 1999, Ion microprobe analysis of oxygen isotope ratios in granulite facies magnetites: diffusive exchange as a guide to cooling history: Contributions to Mineralogy and Petrology, v. 109, p. 38-52.

Whitehouse, M.J., 2004, Multi-collector SIMS analysis of trace lanthanides in zircon ($ZrSiO_4$): Geostandards and Geoanalytical Research, v. 28, p.195-201.

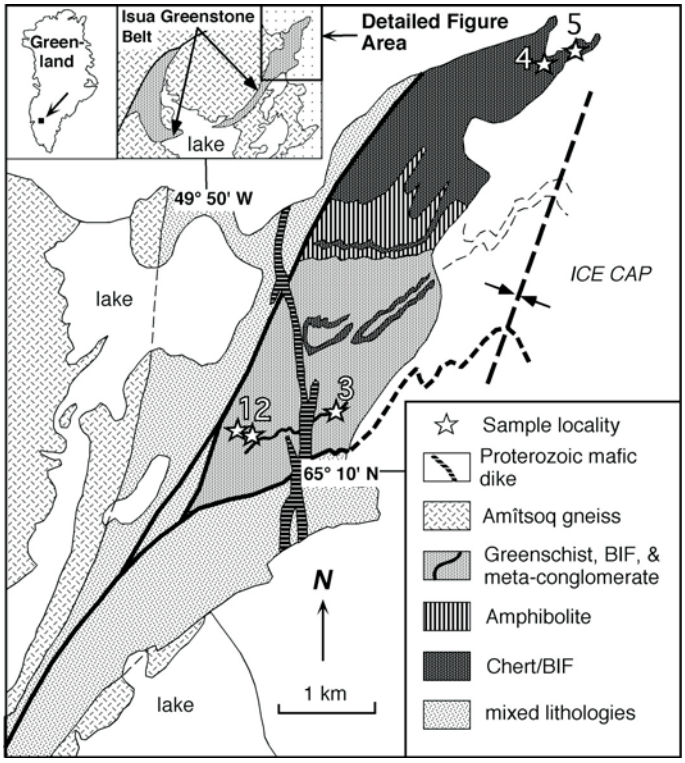

Figure DR1. Map showing the location of the Isua Greenstone Belt and the lithologic distribution in the northeastern sector. Sample locations used in this study are numbered 1 - 5, where 1 = IS-01-05, 2 = IS-02-06, 3 = 462622, 4 = IS-02-08, and 5 = 248474.

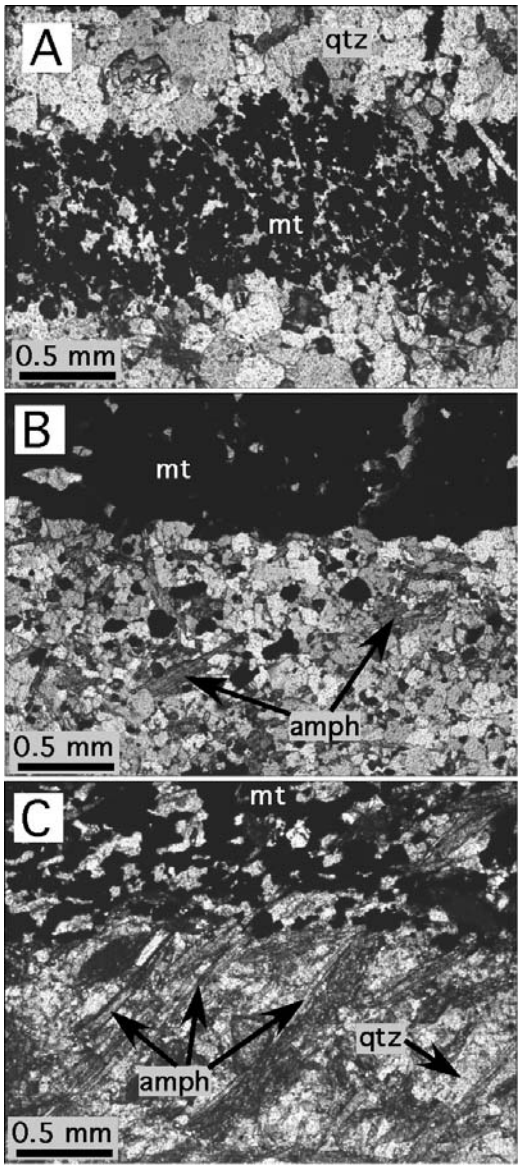

Figure DR2. Plane polarized light photomicrographs of the three variants of BIF from the IGB investigated in this study. Abbreviations: mt = magnetite; qtz = quartz; amph = amphibole. (A) Sample IS-02-08 consists of alternating mm-scale bands of quartz and magnetite. (B) Sample IS-02-06 consists predominantly of alternating mm-scale bands of quartz and magnetite with disseminated green amphibole the quartz-rich bands. (C) Sample IS-02-05 consists of alternating mm-scale bands of magnetite and amphibole with less common disseminated quartz in both bands.

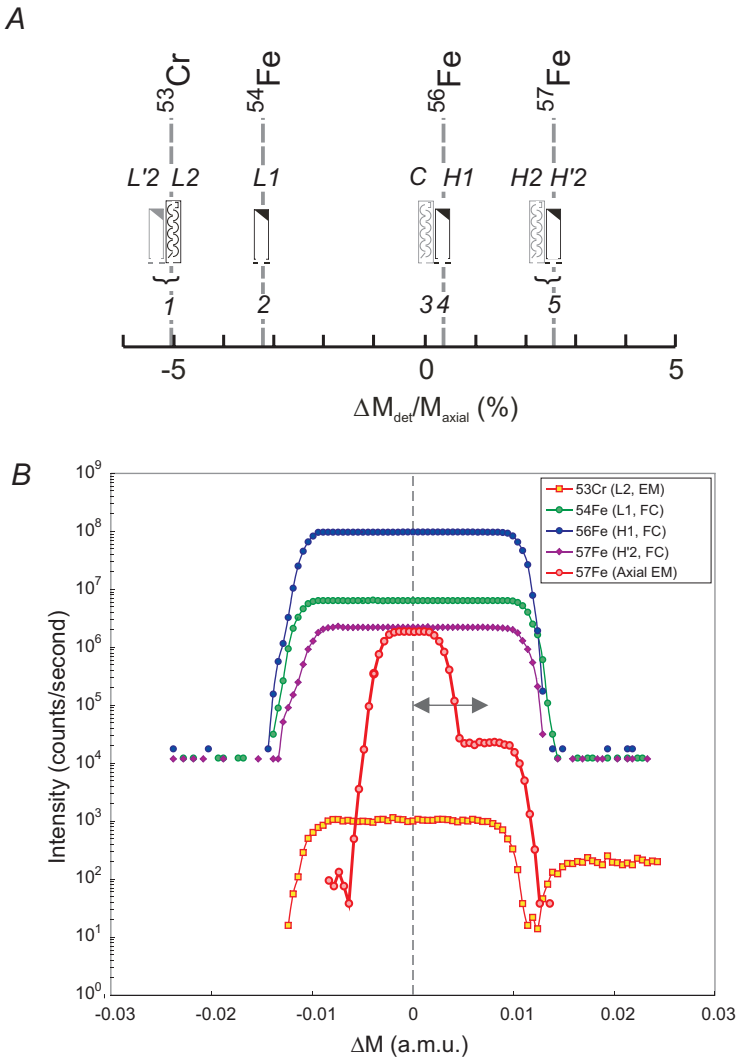

Figure DR3. (a) Placement of detectors used for this study along the focal plane of the Cameca IMS1270 multicollector SIMS. Detectors shown in grey were not utilized. Italicized numbers refer to the moving trolley designation (1, 2, etc…) and detector names (L'2, L2, L1, etc…). (b) Actual scan of Fe signal from magnetite showing detector coincidence, quality of peak shape and peak flatness. Superimposed on the low mass resolution scans is a high mass resolution (MRP ca. 8000) scan of the ^{57}Fe peak made with the axial EM detector; the low noise level of the EM detector and high mass resolution reveals the ^{56}Fe^{1}H peak to the high mass side of ^{57}Fe; the magnitude of the hydride peak is about 1% of the ^{57}Fe peak and therefore represents a ca. 0.2 ‰ level of hydride formation. Horizontal arrow indicates displacement of the ^{56}Fe^{1}H peak from the axis; for actual analysis, the H'2 FC detector was moved to high mass by this amount to ensure that measurement was made on the part of the compound low mass resolution peak that is only ^{57}Fe.

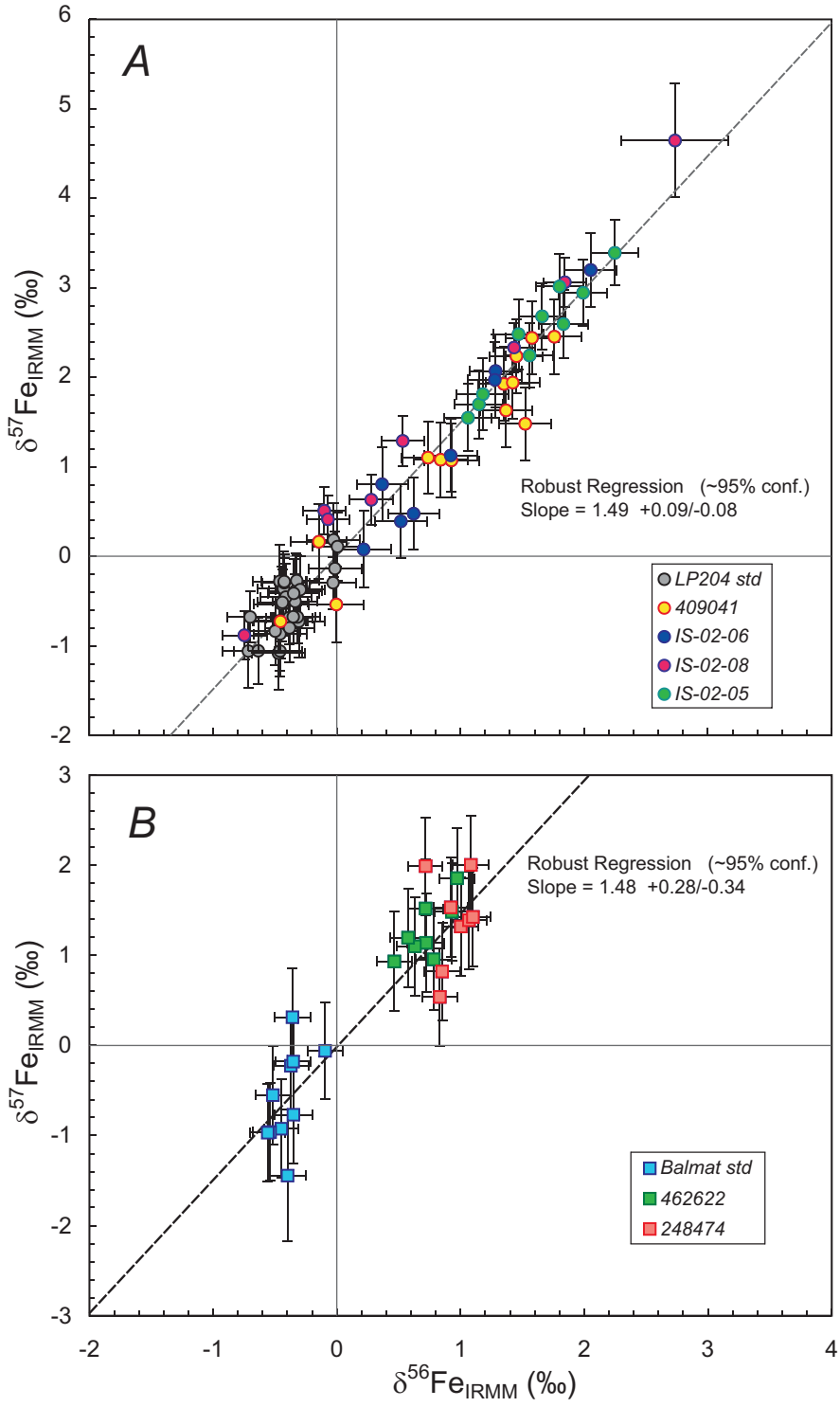

Figure DR4. Correlation plots of $\delta^{57}Fe$ against $\delta^{56}Fe$ for (a) magnetite and (b) pyrite analyses. Robust regression calculations indicate that data lie on the expected mass dependent fractionation trend. Error bars are $1\sigma_{ext}$ for the relevant session.

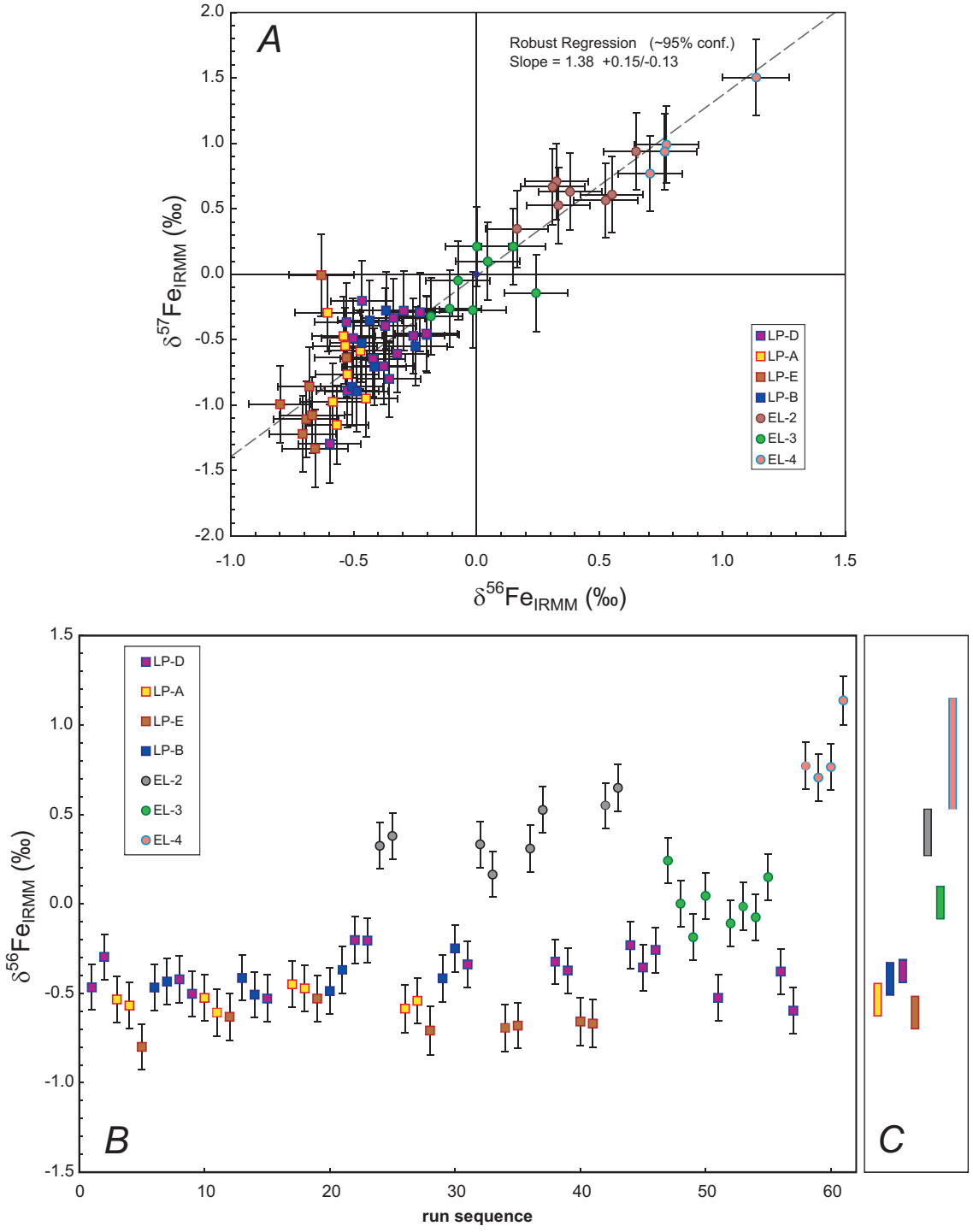

Figure DR5. Plot of results from homogeneity tests on magnetite references. (a) Correlation plot of $\delta^{57}Fe$ against $\delta^{56}Fe$ for data obtained during magnetite homogenization test; error bars are $1\sigma_{ext}$. (b) Time sequenced plot of $\delta^{56}Fe$ from four crystals of magnetite LP-204 (LP-A, LP-B, LP-D and LP-E) and three crystals of magnetite from El Laco, Chile (EL-2, EL-3 and EL-4). LP-204 crystal LP-D was used as the calibration standard assuming $\delta^{56}Fe$ = -0.375 ‰; error bars are $1\sigma_{ext}$ for the relevant session. (c) weighted average of $\delta^{56}Fe$ from each crystal (color coding as in (b)); error bars are 95% confidence.

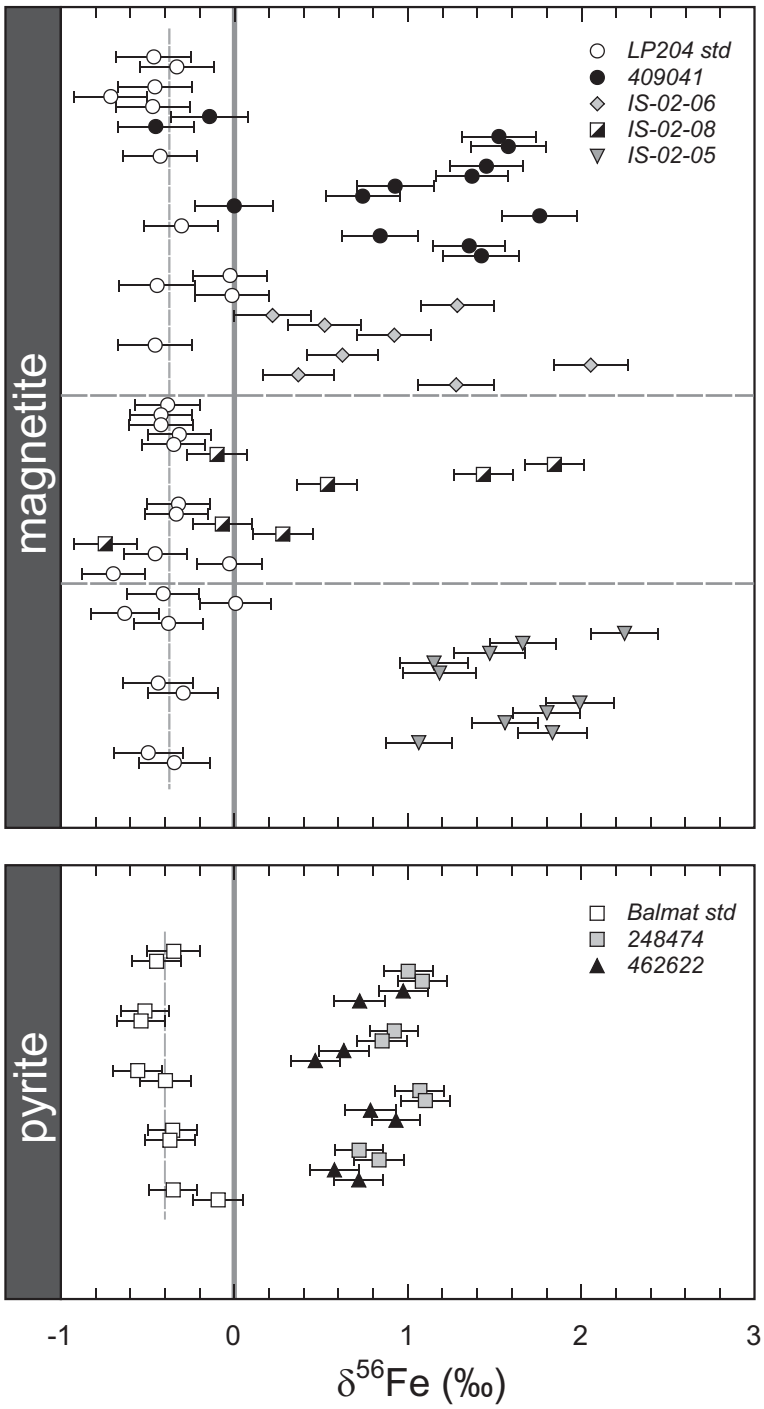

Figure DR6. Diagram plots δ^{56}Fe values (in ‰) for magnetite and pyrite from IGB samples. Data are presented in original run sequence interspersed with standard analyses: LP-204 magnetite, δ^{56}Fe = -0.375 ‰ and Balmat pyrite, δ^{56}Fe = -0.399 ‰ (reference compositions of the two standards are shown as dashed vertical lines). Dashed horizontal lines separate analytical sessions for magnetite; pyrite analyses were performed in a single session. Error bars are shown at ± 1σ and include the propagated external uncertainty from the standard measurements for each session.

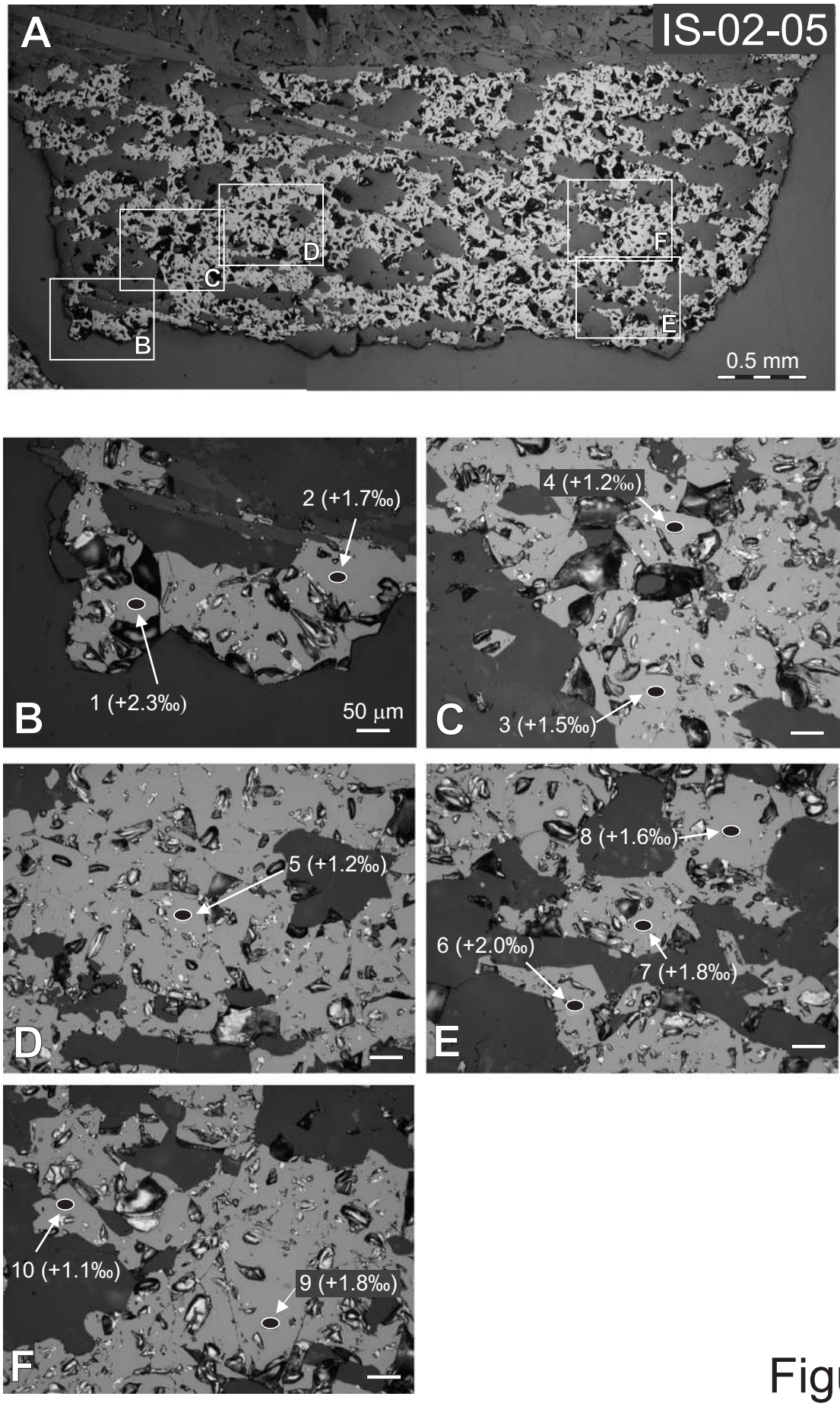
A
IS-02-05
B
C
D
E
F
0.5 mm
2 (+1.7‰)
1 (+2.3‰)
B
50 μm
4 (+1.2‰)
3 (+1.5‰)
C
5 (+1.2‰)
D
8 (+1.6‰)
6 (+2.0‰)
7 (+1.8‰)
E
10 (+1.1‰)
9 (+1.8‰)
F

Figure 7A

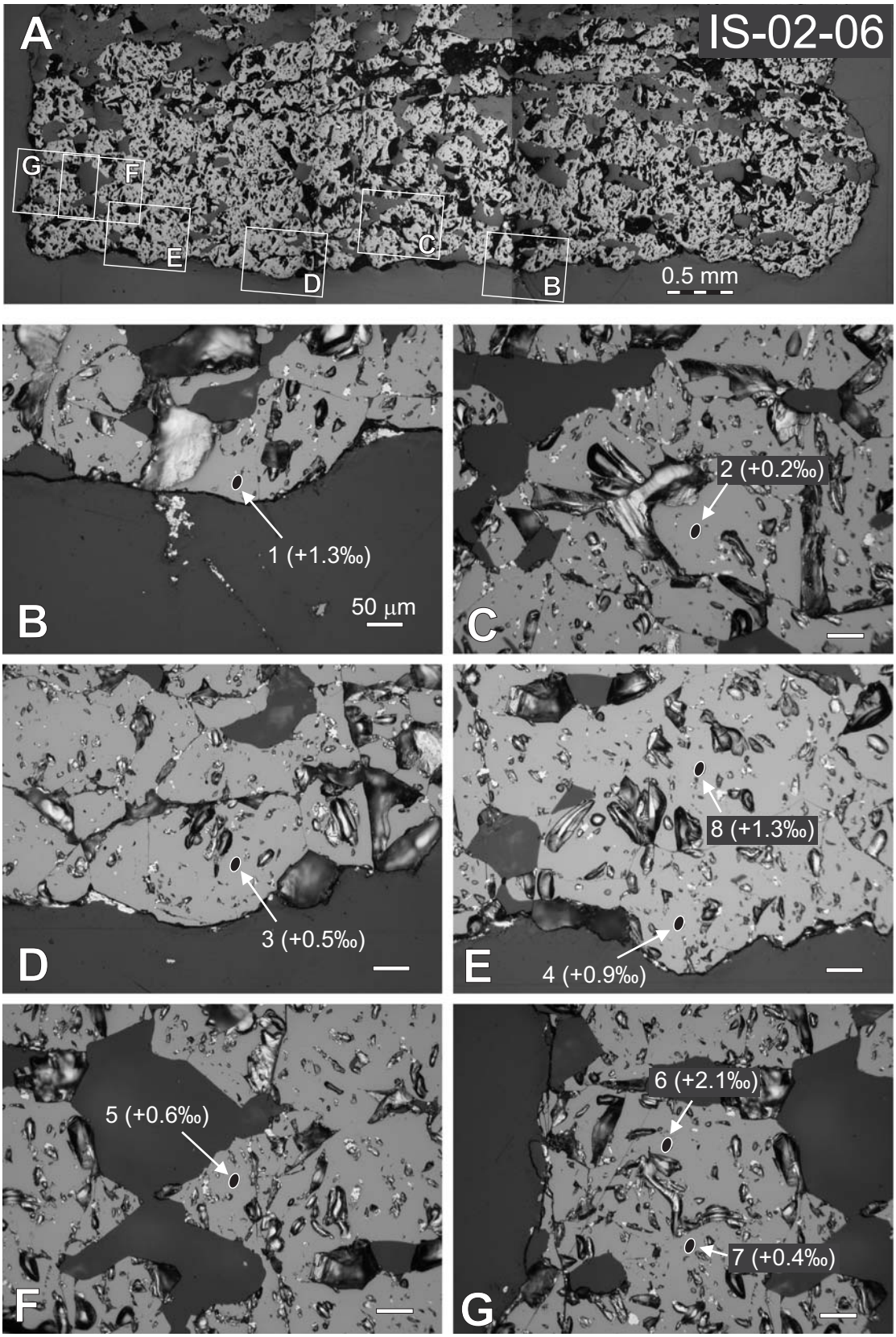
A
IS-02-06
G
F
E
D
C
B
0.5 mm
1 (+1.3‰)
50 µm
B
2 (+0.2‰)
C
3 (+0.5‰)
D
8 (+1.3‰)
4 (+0.9‰)
E
5 (+0.6‰)
F
6 (+2.1‰)
7 (+0.4‰)
G

Figure 7B

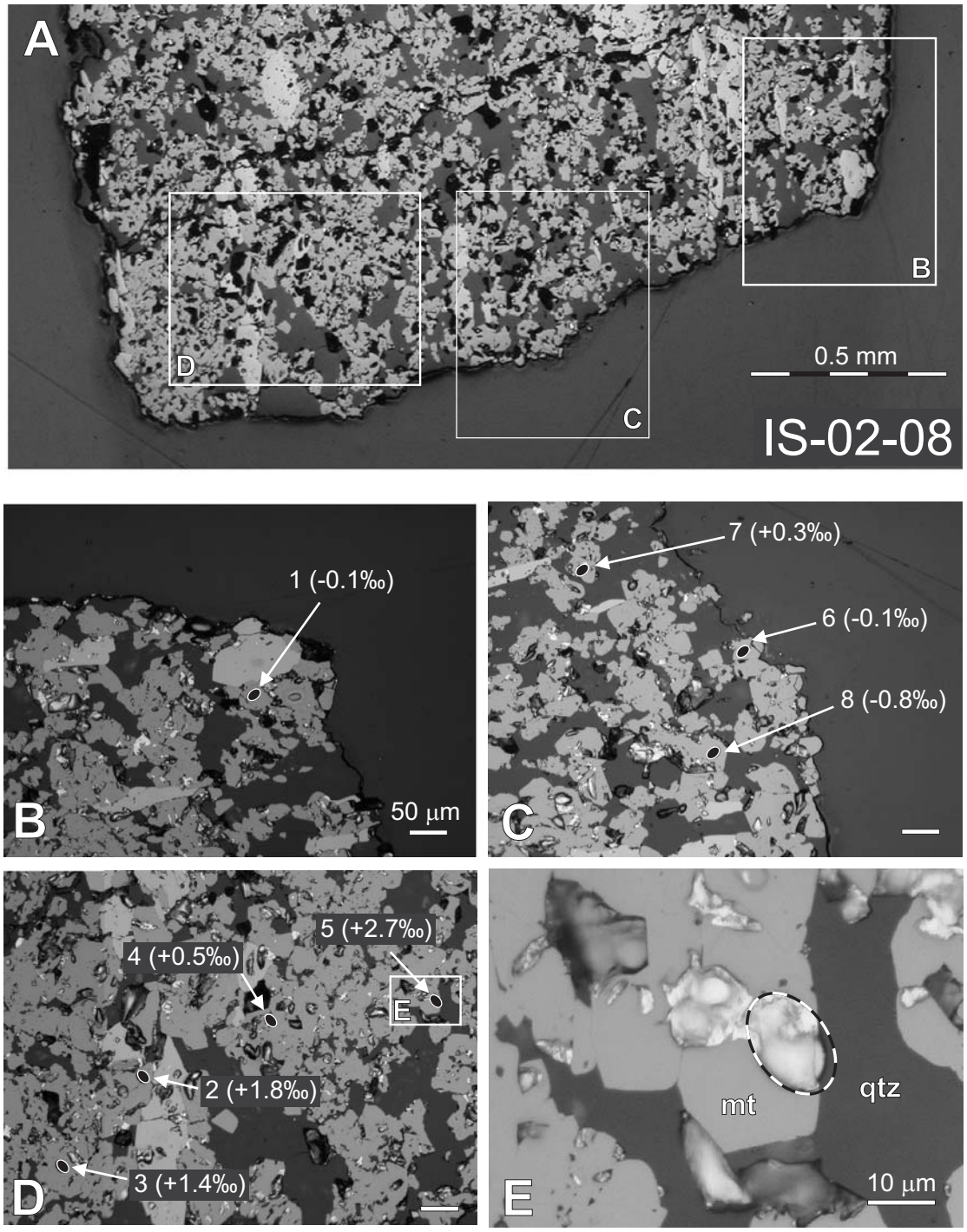
A
B
C
D
0.5 mm
IS-02-08
1 (-0.1‰)
50 µm
B
7 (+0.3‰)
6 (-0.1‰)
8 (-0.8‰)
C
5 (+2.7‰)
4 (+0.5‰)
E
2 (+1.8‰)
3 (+1.4‰)
D
mt
qtz
10 µm
E

Figure 7C

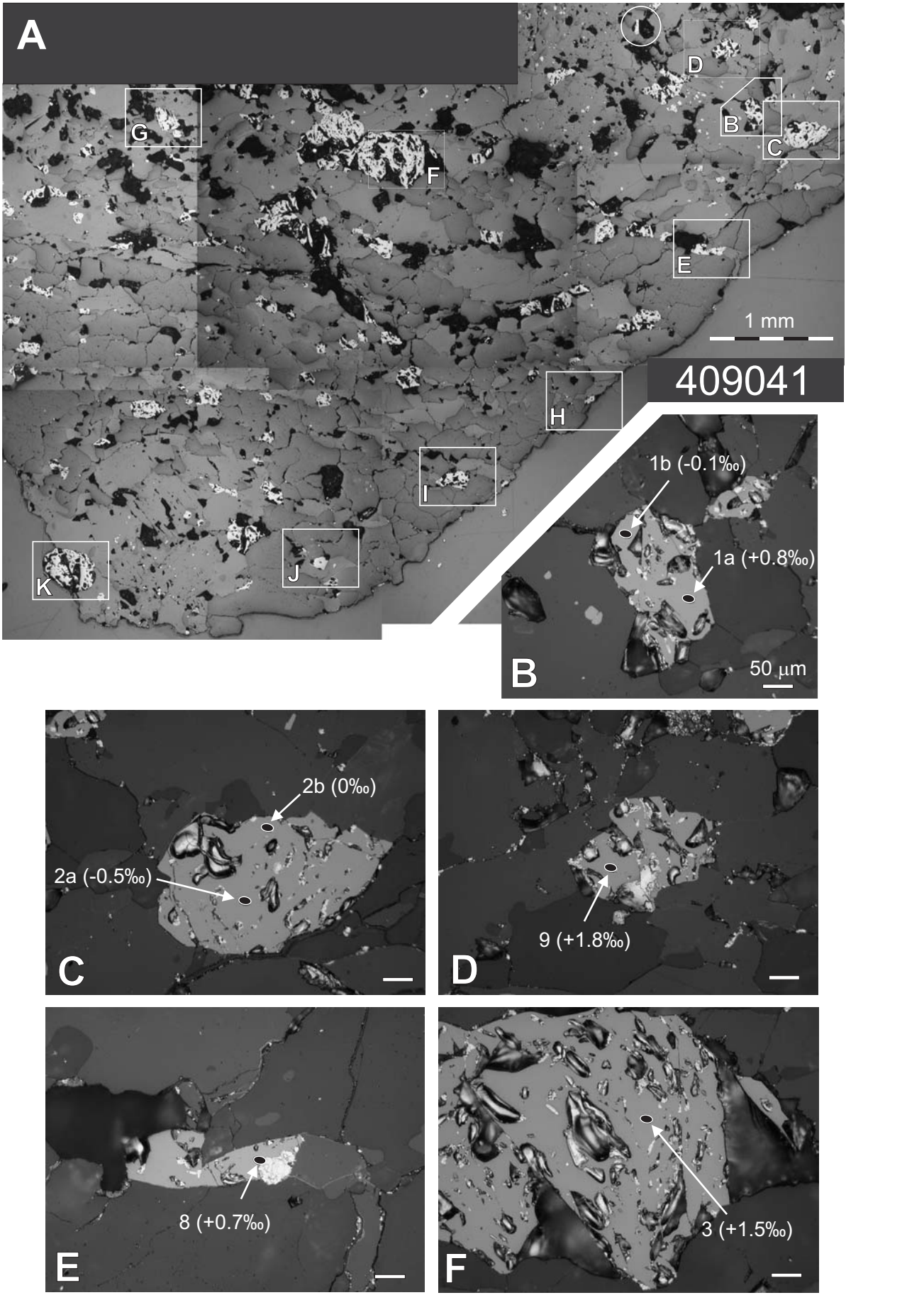
A
D
B
C
G
F
E
1 mm
409041
H
I
J
K
1b (-0.1‰)
1a (+0.8‰)
B
50 μm
2b (0‰)
2a (-0.5‰)
C
9 (+1.8‰)
D
8 (+0.7‰)
E
3 (+1.5‰)
F

Figure 7D

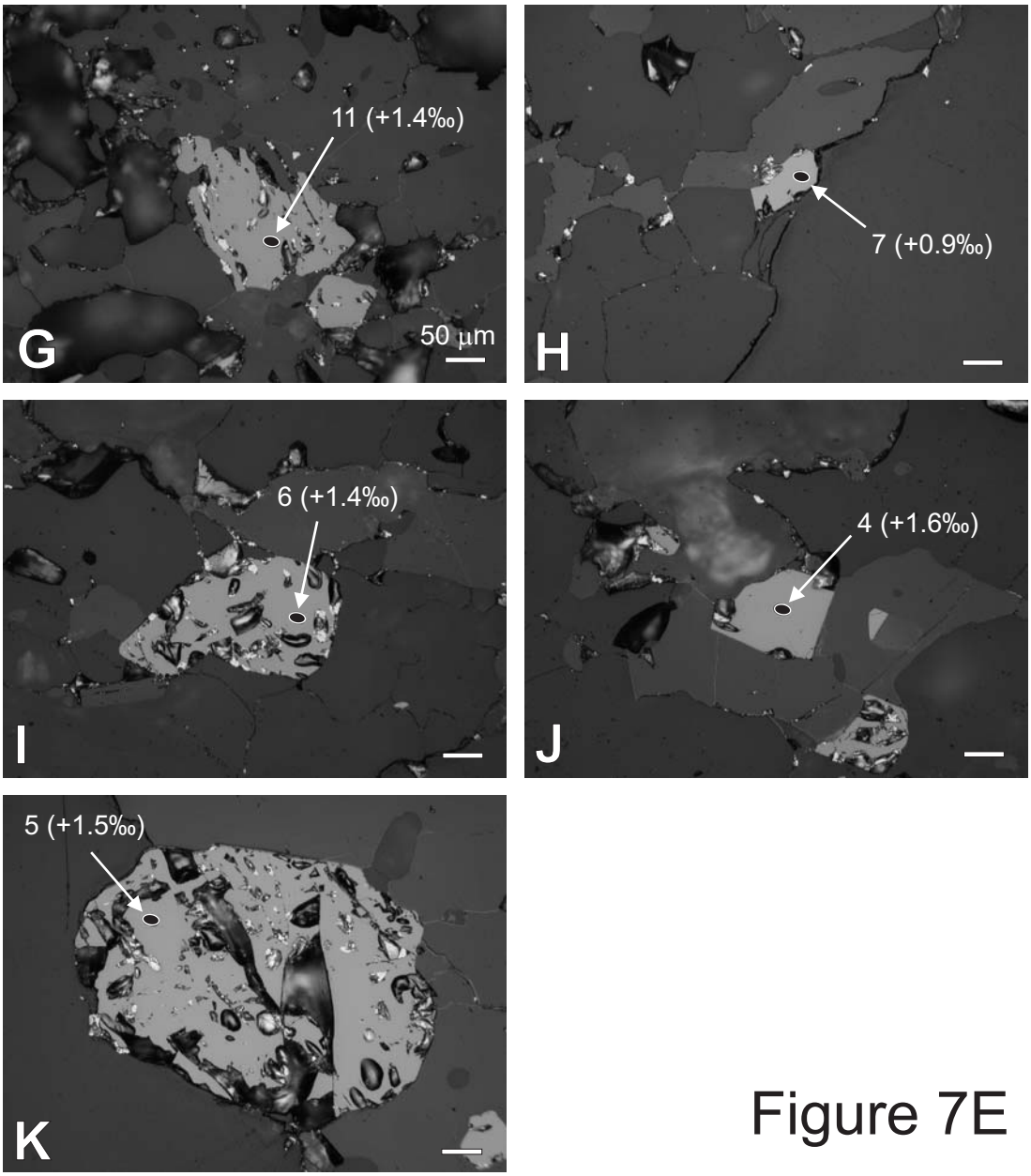

Figure 7E

Figure DR7. Reflected light microscope images of analysis locations, annotated with the obtained δ^{56}Fe values corresponding to analysis number in Table DR2. Note that due to differential polishing of softer magnetite relative to quartz, some flakes of the removed gold coating have collected on the magnetites. These could not be removed without risk of polishing away analytical craters. (a) Sample IS-02-05; (b) Sample IS-02-06; (c) Sample IS-02-08; note higher magnification image of spot 5 (panel E) showing slight overlap of analytical crater onto quartz; (d) and (e) Sample 409041.

Table DR1: Fe isotope composition of SIMS reference materials run by MC-ICP-MS

Sample	Matrix type	δ^{56}Fe	±	[a]2σ	δ^{57}Fe	±	[a]2σ	δ^{58}Fe	±	[a]2σ
LP-204 – run 1	magnetite	-0.393	±	45	-0.570	±	85	-0.65	±	55
LP-204 – run 2	magnetite	-0.358	±	51	-0.514	±	88	-0.45	±	79
	average	*-0.376*	±	*49*	*-0.542*	±	*79*	*-0.55*	±	*0.28*
LS68 – run 1	magnetite	0.247	±	46	0.363	±	84	0.93	±	65
LS68 – run 2	magnetite	0.275	±	46	0.383	±	94	0.55	±	77
	average	*0.261*	±	*46*	*0.373*	±	*89*	*0.74*	±	*71*
Balmat – run 1	pyrite	-0.39	±	46	-0.578	±	93	-0.44	±	62
Balmat – run 2	pyrite	-0.409	±	61	-0.576	±	92	-0.71	±	67
	average	*-0.649*	±	*54*	*-0.888*	±	*93*	*-1.28*	±	*77*
248474 – run 1	pyrite	0.954	±	40	1.438	±	76	1.96	±	63
248474 – run 2	pyrite	0.914	±	46	1.417	±	93	1.67	±	84
	average	*0.934*	±	*43*	*1.428*	±	*84*	*1.81*	±	*73*
JM long term grand average	*(n = 1014)*	*0.424*	±	*47*[b]	*0.627*	±	*77*[b]	*0.83*	±	*43*[b]

[a] 2 standard deviation internal uncertainty measured during the run

[b] 2 standard deviation external

Table DR2. Fe isotope data for Isua samples and associated standard runs

Filename	Mineral	Session.run[a]	^{56}Fe cps x 10^6	$^{56}Fe/^{54}Fe$ raw	±σ	$^{57}Fe/^{54}Fe$ raw	±σ	$^{53}Cr/^{54}Fe$ raw[b]	±σ	Drift corr.[c]	$^{56}Fe/^{54}Fe$ corr.[d]	$^{57}Fe/^{54}Fe$ corr.[d]	$\delta^{56}Fe$[e] (‰)	±σ	$\delta^{57}Fe$[e] (‰)	±σ
LP-204 magnetite (reference: $\delta^{56}Fe$ = -0.375 ‰)																
LP-ISB	mt	1.1	178.4	15.2392	0.0011	0.346472	0.000036	0.00016424	0.00000024	no	15.2398	0.346487	-0.47	0.21	-0.72	0.41
LP-ISB@4	mt	1.2	181.6	15.2412	0.0009	0.346589	0.000044	0.00016206	0.00000024	no	15.2419	0.346603	-0.33	0.21	-0.38	0.41
LP-ISB@6	mt	1.4	186.2	15.2393	0.0010	0.346625	0.000039	0.00016059	0.00000024	no	15.2399	0.346640	-0.46	0.21	-0.28	0.41
LP-ISB@7	mt	1.5	185.9	15.2354	0.0009	0.346355	0.000041	0.00016492	0.00000024	no	15.2361	0.346370	-0.71	0.21	-1.06	0.41
LP-ISB@8	mt	1.6	186.9	15.2391	0.0010	0.346347	0.000039	0.00016409	0.00000024	no	15.2398	0.346362	-0.47	0.21	-1.08	0.41
LP-ISB@9	mt	1.11	188.1	15.2398	0.0010	0.346596	0.000042	0.00016334	0.00000024	no	15.2404	0.346611	-0.43	0.21	-0.36	0.41
LP-ISB@11	mt	1.18	189.8	15.2416	0.0010	0.346470	0.000038	0.00016319	0.00000023	no	15.2423	0.346485	-0.31	0.21	-0.73	0.41
LP-ISB@12	mt	1.22	173.4	15.2519	0.0012	0.346823	0.000041	0.00016110	0.00000026	no	*omitted as outlier*					
LP-ISB@13	mt	1.23	171.5	15.2459	0.0011	0.346785	0.000042	0.00016274	0.00000025	no	15.2466	0.346800	-0.03	0.21	0.18	0.41
LP-ISB@14	mt	1.24	163.7	15.2395	0.0013	0.346538	0.000047	0.00016323	0.00000025	no	15.2402	0.346552	-0.45	0.22	-0.53	0.42
LP-ISB@15	mt	1.25	174.3	15.2461	0.0011	0.346674	0.000039	0.00016180	0.00000024	no	15.2467	0.346689	-0.01	0.21	-0.14	0.41
LP-ISB@16	mt	1.30	120.4	15.2393	0.0010	0.346421	0.000045	0.00016399	0.00000029	no	15.2400	0.346436	-0.46	0.21	-0.87	0.41
LP-ISB@19	mt	2.1	140.9	15.2294	0.0014	0.345998	0.000047	0.00016797	0.00000035	0.068, 0.106	15.2301	0.346013	-0.39	0.19	-0.69	0.29
LP-ISB@20	mt	2.2	139.6	15.2298	0.0011	0.346170	0.000037	0.00016754	0.00000031	0.068, 0.106	15.2295	0.346148	-0.42	0.18	-0.30	0.28
LP-ISB@21	mt	2.3	142.3	15.2309	0.0012	0.346211	0.000054	0.00016745	0.00000046	0.068, 0.106	15.2295	0.346153	-0.42	0.18	-0.28	0.30
LP-ISB@22	mt	2.4	141.5	15.2335	0.0011	0.346111	0.000047	0.00016666	0.00000028	0.068, 0.106	15.2311	0.346016	-0.32	0.18	-0.68	0.29
LP-ISB@23	mt	2.5	140.9	15.2340	0.0011	0.346149	0.000048	0.00016665	0.00000038	0.068, 0.106	15.2306	0.346017	-0.35	0.18	-0.67	0.29
LP-ISB@24	mt	2.11	134.3	15.2406	0.0011	0.346509	0.000038	0.00016564	0.00000034	0.068, 0.106	15.2310	0.346156	-0.32	0.18	-0.27	0.28
LP-ISB@25	mt	2.12	133.8	15.2415	0.0012	0.346466	0.000053	0.00016534	0.00000034	0.068, 0.106	15.2308	0.346076	-0.34	0.18	-0.50	0.30
LP-ISB@26	mt	2.16	128.3	15.2438	0.0012	0.346421	0.000043	0.00016485	0.00000041	0.068, 0.106	15.2290	0.345884	-0.46	0.18	-1.06	0.29
LP-ISB@27	mt	2.17	127.0	15.2513	0.0013	0.346721	0.000046	0.00016460	0.00000040	0.068, 0.106	15.2355	0.346148	-0.03	0.19	-0.30	0.29
LP-ISB@28	mt	2.18	130.2	15.2421	0.0012	0.346626	0.000042	0.00016459	0.00000040	0.068, 0.106	15.2253	0.346016	-0.70	0.18	-0.68	0.29
LP_ISB@43	mt	3.1	153.6	15.2380	0.0014	0.346405	0.000041	0.00016480	0.00000037	0.056, 0.092	15.2387	0.346420	-0.41	0.21	-0.45	0.38
LP_ISB@44	mt	3.2	153.8	15.2452	0.0013	0.346632	0.000047	0.00016388	0.00000030	0.056, 0.092	15.2450	0.346615	0.01	0.20	0.11	0.38
LP_ISB@45	mt	3.3	154.5	15.2363	0.0010	0.346261	0.000035	0.00016184	0.00000036	0.056, 0.092	15.2353	0.346212	-0.63	0.20	-1.06	0.37
LP_ISB@46	mt	3.4	156.0	15.2410	0.0012	0.346381	0.000045	0.00016272	0.00000026	0.056, 0.092	15.2391	0.346300	-0.38	0.20	-0.80	0.38
LP_ISB@47	mt	3.10	160.3	15.2452	0.0012	0.346672	0.000039	0.00016321	0.00000028	0.056, 0.092	15.2382	0.346399	-0.44	0.20	-0.52	0.37
LP_ISB@48	mt	3.11	159.5	15.2483	0.0012	0.346754	0.000043	0.00016276	0.00000027	0.056, 0.092	15.2404	0.346448	-0.30	0.20	-0.37	0.38
LP_ISB@49	mt	3.17	159.6	15.2503	0.0012	0.346785	0.000045	0.00016290	0.00000029	0.056, 0.092	15.2374	0.346288	-0.50	0.20	-0.83	0.38
LP_ISB@50	mt	3.18	163.0	15.2534	0.0014	0.346963	0.000044	0.00016173	0.00000026	0.056, 0.092	15.2396	0.346434	-0.35	0.21	-0.41	0.38
409041 (banded quartz-pyroxene lithology, south of Isua; GPS N65°01.03' W050°12.20')																
SM-00-41_Fe@1	mt	1.7	161.9	15.2440	0.0014	0.346775	0.000046	0.00019622	0.00000092	no	15.2448	0.346793	-0.14	0.22	0.16	0.42
SM-00-41_Fe@2	mt	1.8	150.2	15.2395	0.0013	0.346472	0.000042	0.00014436	0.00000025	no	15.2400	0.346485	-0.45	0.22	-0.73	0.41
SM-00-41_Fe@3	mt	1.9	162.6	15.2696	0.0009	0.347236	0.000037	0.00014981	0.00000025	no	15.2702	0.347249	1.52	0.21	1.48	0.41
SM-00-41_Fe@4	mt	1.10	174.4	15.2709	0.0011	0.347580	0.000039	0.00002687	0.00000010	no	15.2710	0.347583	1.58	0.22	2.44	0.41
SM-00-41_Fe@5	mt	1.12	173.3	15.2690	0.0010	0.347508	0.000037	0.00003409	0.00000013	no	15.2691	0.347512	1.45	0.21	2.24	0.41
SM-00-41_Fe@6	mt	1.13	171.2	15.2675	0.0008	0.347293	0.000033	0.00008711	0.00000018	no	15.2678	0.347301	1.37	0.21	1.63	0.41
SM-00-41_Fe@7	mt	1.14	153.6	15.2610	0.0014	0.347106	0.000045	0.00002070	0.00000044	no	15.2611	0.347108	0.93	0.22	1.07	0.41
SM-00-41_Fe@8	mt	1.15	177.4	15.2581	0.0011	0.347116	0.000034	0.00003075	0.00000017	no	15.2582	0.347119	0.74	0.22	1.10	0.41
SM-00-41_Fe@2b	mt	1.16	154.2	15.2460	0.0014	0.346529	0.000050	0.00023667	0.00000035	no	15.2469	0.346550	0.00	0.22	-0.54	0.42
SM-00-41_Fe@9	mt	1.17	171.2	15.2732	0.0011	0.347575	0.000048	0.00012985	0.00000048	no	15.2738	0.347587	1.76	0.22	2.45	0.42
SM-00-41_Fe@1b	mt	1.19	160.6	15.2592	0.0012	0.347098	0.000047	0.00013124	0.00000146	no	15.2598	0.347110	0.84	0.22	1.08	0.42
SM-00-41_Fe@10	mt	1.20	157.7	15.2670	0.0007	0.347390	0.000045	0.00015025	0.00000035	no	15.2676	0.347404	1.35	0.21	1.93	0.41
SM-00-41_Fe@11	mt	1.21	161.9	15.2682	0.0012	0.347400	0.000033	0.00010522	0.00000042	no	15.2687	0.347409	1.42	0.22	1.94	0.41
IS-02-06 (BIF, Isua Greenstone Belt; N65°10.323' W049°49.200')																
0206_Fe@1	mt	1.26	142.8	15.2662	0.0007	0.347447	0.000039	0.00007260	0.00000021	no	15.2665	0.347454	1.28	0.21	2.07	0.41
0206_Fe@2	mt	1.27	124.0	15.2501	0.0013	0.346758	0.000059	0.00005620	0.00000017	no	15.2503	0.346763	0.22	0.22	0.08	0.43

continued next page

Table DR2 continued

Filename	Mineral	Session.run[a]	^{56}Fe	$^{56}Fe/^{54}Fe$	±σ	$^{57}Fe/^{54}Fe$	±σ	$^{53}Cr/^{54}Fe$	±σ	Drift corr.[c]	$^{56}Fe/^{54}Fe$	$^{57}Fe/^{54}Fe$	$\delta^{56}Fe$[e]	±σ	$\delta^{57}Fe$[e]	±σ
			cps x 10^6	raw		raw		raw[b]			corr.[d]	corr.[d]	(‰)		(‰)	
0206_Fe@3	mt	1.28	128.0	15.2546	0.0008	0.346865	0.000044	0.00007501	0.00000022	no	15.2549	0.346872	0.52	0.21	0.39	0.41
0206_Fe@4	mt	1.29	119.1	15.2607	0.0010	0.347120	0.000034	0.00006937	0.00000020	no	15.2610	0.347127	0.92	0.21	1.13	0.41
0206_Fe@5	mt	1.31	100.9	15.2562	0.0005	0.346897	0.000024	0.00005297	0.00000018	no	15.2564	0.346902	0.62	0.21	0.48	0.40
0206_Fe@6	mt	1.32	106.3	15.2780	0.0009	0.347840	0.000043	0.00006339	0.00000019	no	15.2782	0.347845	2.05	0.21	3.20	0.41
0206_Fe@7	mt	1.33	92.0	15.2522	0.0006	0.347007	0.000039	0.00009717	0.00000026	no	15.2526	0.347015	0.37	0.21	0.81	0.41
0206_Fe@8	mt	1.34	143.3	15.2661	0.0013	0.347412	0.000053	0.00008620	0.00000020	no	15.2664	0.347420	1.28	0.22	1.97	0.42
IS-02-08 (BIF, Isua Greenstone Belt; N 65°12.531' W049°45.504')																
IM_Fe@1	mt	2.6	130.1	15.2395	0.0007	0.346610	0.000025	0.00001329	0.00000009	0.068, 0.106	15.2344	0.346427	-0.10	0.17	0.51	0.27
IM_Fe@2	mt	2.7	115.5	15.2702	0.0007	0.347530	0.000034	0.00001155	0.00000008	0.068, 0.106	15.2640	0.347310	1.84	0.17	3.06	0.28
IM_Fe@3	mt	2.8	133.8	15.2649	0.0006	0.347314	0.000030	0.00001153	0.00000008	0.068, 0.106	15.2578	0.347058	1.43	0.17	2.33	0.27
IM_Fe@4	mt	2.9	128.1	15.2523	0.0008	0.346990	0.000034	0.00001294	0.00000009	0.068, 0.106	15.2441	0.346697	0.53	0.17	1.29	0.28
IM_Fe@5	mt	2.10	117.7	15.2868	0.0061	0.348188	0.000200	0.00001247	0.00000013	0.068, 0.106	15.2776	0.347859	2.73	0.43	4.65	0.63
IM_Fe@6	mt	2.13	124.0	15.2472	0.0007	0.346833	0.000024	0.00001315	0.00000008	0.068, 0.106	15.2349	0.346393	-0.07	0.17	0.41	0.27
IM_Fe@7	mt	2.14	124.6	15.2535	0.0008	0.346946	0.000041	0.00001297	0.00000008	0.068, 0.106	15.2402	0.346469	0.28	0.17	0.63	0.29
IM_Fe@8	mt	2.15	128.6	15.2390	0.0011	0.346459	0.000031	0.00001308	0.00000008	0.068, 0.106	15.2246	0.345945	-0.75	0.18	-0.88	0.27
IS-02-05 (BIF, Isua Greenstone Belt; N 65°10.350' W049°49.263')																
CM_Fe@1	mt	3.5	144.7	15.2825	0.0008	0.347879	0.000027	0.00001397	0.00000011	0.056, 0.092	15.2792	0.347752	2.25	0.19	3.39	0.37
CM_Fe@2	mt	3.6	141.4	15.2744	0.0007	0.347664	0.000035	0.00002228	0.00000010	0.056, 0.092	15.2702	0.347506	1.66	0.19	2.68	0.37
CM_Fe@3	mt	3.7	140.4	15.2724	0.0014	0.347628	0.000054	0.00001337	0.00000008	0.056, 0.092	15.2673	0.347437	1.47	0.21	2.48	0.39
CM_Fe@4	mt	3.8	143.3	15.2683	0.0009	0.347388	0.000043	0.00001818	0.00000009	0.056, 0.092	15.2625	0.347166	1.15	0.19	1.70	0.38
CM_Fe@5	mt	3.9	133.4	15.2695	0.0015	0.347456	0.000065	0.00005409	0.00000021	0.056, 0.092	15.2629	0.347205	1.18	0.21	1.81	0.40
CM_Fe@6	mt	3.12	152.5	15.2845	0.0009	0.347947	0.000034	0.00002431	0.00000010	0.056, 0.092	15.2753	0.347597	1.99	0.20	2.95	0.37
CM_Fe@7	mt	3.13	137.6	15.2824	0.0008	0.348003	0.000029	0.00002932	0.00000012	0.056, 0.092	15.2724	0.347622	1.80	0.19	3.01	0.37
CM_Fe@8	mt	3.14	142.7	15.2797	0.0008	0.347771	0.000019	0.00000624	0.00000005	0.056, 0.092	15.2687	0.347355	1.56	0.19	2.25	0.36
CM_Fe@9	mt	3.15	145.7	15.2847	0.0012	0.347924	0.000044	0.00000680	0.00000005	0.056, 0.092	15.2728	0.347476	1.83	0.20	2.60	0.38
CM_Fe@10	mt	3.16	146.9	15.2738	0.0007	0.347593	0.000038	0.00000915	0.00000006	0.056, 0.092	15.2611	0.347114	1.06	0.19	1.55	0.37
Balmat pyrite (reference: $\delta^{56}Fe$ = -0.399 ‰)																
Bal_CF-pyr-01	py	4.1	94.4	15.1705	0.0011	0.343996	0.000039			no	15.1705	0.343996	-0.35	0.15	-0.77	0.54
Bal_CF-pyr-02	py	4.2	96.1	15.1690	0.0006	0.343943	0.000042			no	15.1690	0.343943	-0.45	0.14	-0.92	0.55
Bal_CF-pyr-03	py	4.7	94.9	15.1680	0.0006	0.344071	0.000037			no	15.1680	0.344071	-0.52	0.14	-0.55	0.54
Bal_CF-pyr-04	py	4.8	94.6	15.1677	0.0006	0.343930	0.000037			no	15.1677	0.343930	-0.54	0.14	-0.96	0.54
Bal_CF-pyr-05	py	4.13	91.5	15.1674	0.0007	0.343927	0.000039			no	15.1674	0.343927	-0.56	0.14	-0.97	0.54
Bal_CF-pyr-06	py	4.14	92.2	15.1698	0.0010	0.343763	0.000172			no	15.1698	0.343763	-0.40	0.15	-1.44	0.73
Bal_CF-pyr-07	py	4.19	92.0	15.1704	0.0008	0.344368	0.000030			no	15.1704	0.344368	-0.36	0.14	0.31	0.54
Bal_CF-pyr-08	py	4.20	91.5	15.1702	0.0007	0.344182	0.000037			no	15.1702	0.344182	-0.37	0.14	-0.23	0.54
Bal_CF-pyr-09	py	4.25	91.6	15.1705	0.0006	0.344198	0.000040			no	15.1705	0.344198	-0.35	0.14	-0.18	0.54
Bal_CF-pyr-10	py	4.26	89.6	15.1744	0.0008	0.344240	0.000026			no	15.1744	0.344240	-0.09	0.14	-0.06	0.54
248474 (BIF, Isua Greenstone Belt; reference $\delta^{56}Fe$ = 0.954 ‰; GPS N65°12.653' W049°45.168'W)																
248474_CF-pyr_01	py	4.3	95.7	15.1911	0.0007	0.344715	0.000039			no	15.1911	0.344715	1.00	0.14	1.32	0.54
248474_CF-pyr_02	py	4.4	92.8	15.1923	0.0008	0.344949	0.000034			no	15.1923	0.344949	1.08	0.14	2.00	0.54
248474_CF-pyr_03	py	4.9	94.2	15.1898	0.0005	0.344787	0.000049			no	15.1898	0.344787	0.92	0.14	1.53	0.55
248474_CF-pyr_04	py	4.10	93.8	15.1888	0.0008	0.344542	0.000038			no	15.1888	0.344542	0.85	0.14	0.82	0.54
248474_CF-pyr_05	py	4.15	92.6	15.1921	0.0007	0.344738	0.000037			no	15.1921	0.344738	1.07	0.14	1.39	0.54
248474_CF-pyr_06	py	4.16	94.3	15.1925	0.0007	0.344751	0.000040			no	15.1925	0.344751	1.10	0.14	1.43	0.55
248474_CF-pyr_07	py	4.21	89.0	15.1867	0.0005	0.344945	0.000034			no	15.1867	0.344945	0.72	0.14	1.99	0.54
248474_CF-pyr_08	py	4.22	88.6	15.1885	0.0007	0.344445	0.000039			no	15.1885	0.344445	0.83	0.14	0.54	0.54
462622 (Conglomerate, Isua Greenstone Belt; GPS N 65°10.466' W049°48.004')																
Cong_01	py	4.5	94.9	15.1906	0.0007	0.344899	0.000047			no	15.1906	0.344899	0.97	0.14	1.86	0.55

continued next page

Table DR2 continued

Filename	Mineral	Session.run[a]	^{56}Fe cps x 10^6	$^{56}Fe/^{54}Fe$ raw	±σ	$^{57}Fe/^{54}Fe$ raw	±σ	$^{53}Cr/^{54}Fe$ raw[b]	±σ	Drift corr.[c]	$^{56}Fe/^{54}Fe$ corr.[d]	$^{57}Fe/^{54}Fe$ corr.[d]	$\delta^{56}Fe$[e] (‰)	±σ	$\delta^{57}Fe$[e] (‰)	±σ
Cong_02	py	4.6	96.2	15.1868	0.0010	0.344652	0.000042			no	15.1868	0.344652	0.72	0.15	1.14	0.55
Cong_03	py	4.11	95.2	15.1854	0.0008	0.344638	0.000044			no	15.1854	0.344638	0.63	0.14	1.10	0.55
Cong_04	py	4.12	93.9	15.1829	0.0006	0.344581	0.000047			no	15.1829	0.344581	0.47	0.14	0.93	0.55
Cong_05	py	4.17	92.4	15.1877	0.0009	0.344589	0.000058			no	15.1877	0.344589	0.78	0.15	0.95	0.56
Cong_06	py	4.18	91.6	15.1900	0.0007	0.344771	0.000037			no	15.1900	0.344771	0.93	0.14	1.48	0.54
Cong_07	py	4.23	90.9	15.1846	0.0008	0.344672	0.000041			no	15.1846	0.344672	0.58	0.14	1.20	0.55
Cong_08	py	4.24	94.4	15.1867	0.0006	0.344783	0.000039			no	15.1867	0.344783	0.72	0.14	1.52	0.54

[a] Refers to analytical session and sequence number in that session (i.e. H-mt1.6 = homogeneity trial, magnetite session1, run number 6)

[b] Omitted where ^{53}Cr count rate is sufficiently low that correction results in <0.01 ‰ correction on $\delta^{56}Fe$.

[c] Indicates whether raw data have been corrected for linear drift within the session and, if so, the magnitude of drift (in ‰/run) for $^{56}Fe/^{54}Fe$ and $^{57}Fe/^{54}Fe$ respectively.

[d] Raw corrected for possible within session drift and interference from ^{54}Cr on ^{54}Fe.

[e] Assumes $\delta^{56}Fe$ = -0.375 ‰ and $\delta^{57}Fe$ = -0.542 ‰ for the LP-204 magnetite grain LP-D; $\delta^{56}Fe$ = -0.399 ‰ and $\delta^{57}Fe$ -0.577 ‰ for Balmat pyrite grain A.

Table DR3. SIMS Fe isotope data from reference sample homogeneity tests

Filename	Mineral	Session.run[a]	^{56}Fe cps x 10^6	^{56}Fe/^{54}Fe raw	±σ	^{57}Fe/^{54}Fe raw	±σ	^{53}Cr/^{54}Fe raw[b]	±σ	Drift corr.[c]	^{56}Fe/^{54}Fe corr.[d]	^{57}Fe/^{54}Fe corr.[d]	δ^{56}Fe[e] (‰)	±σ	δ^{57}Fe[e] (‰)	±σ
LP-204 magnetite (reference: δ^{56}Fe = -0.375 ‰)																
LP-A@1	mt	H-mt1.4	185.9	15.2323	0.0007	0.346436	0.000028	0.00021805	0.00000044	no	15.2332	0.3465	-0.53	0.13	-0.55	0.29
LP-A@2	mt	H-mt1.5	186.9	15.2318	0.0006	0.346226	0.000039	0.00022297	0.00000043	no	15.2326	0.3462	-0.57	0.13	-1.15	0.30
LP-A@3	mt	H-mt1.11	173.3	15.2324	0.0006	0.346361	0.000045	0.00022002	0.00000055	no	15.2333	0.3464	-0.53	0.13	-0.76	0.31
LP-A@4	mt	H-mt1.12	171.2	15.2312	0.0007	0.346524	0.000030	0.00021596	0.00000039	no	15.2321	0.3465	-0.61	0.13	-0.29	0.29
LP-A@5	mt	H-mt1.18	160.6	15.2336	0.0006	0.346297	0.000035	0.00021232	0.00000039	no	15.2345	0.3463	-0.45	0.13	-0.95	0.30
LP-A@6	mt	H-mt1.19	157.7	15.2333	0.0006	0.346424	0.000034	0.00020789	0.00000038	no	15.2341	0.3464	-0.47	0.13	-0.58	0.29
LP-A@7	mt	H-mt1.27	128.0	15.2315	0.0008	0.346288	0.000031	0.00021615	0.00000039	no	15.2324	0.3463	-0.59	0.13	-0.97	0.29
LP-A@8	mt	H-mt1.28	119.1	15.2322	0.0005	0.346462	0.000039	0.00021130	0.00000038	no	15.2331	0.3465	-0.54	0.13	-0.47	0.30
LP-B@1	mt	H-mt1.7	150.2	15.2335	0.0006	0.346446	0.000037	0.00018427	0.00000039	no	15.2342	0.3465	-0.47	0.13	-0.53	0.30
LP-B@2	mt	H-mt1.8	162.6	15.2340	0.0006	0.346506	0.000047	0.00018525	0.00000036	no	15.2347	0.3465	-0.43	0.13	-0.35	0.31
LP-B@3	mt	H-mt1.14	177.4	15.2343	0.0004	0.348270	0.000088	0.00018499	0.00000036	no	15.2350	0.3483	-0.41	0.13	4.74	0.38
LP-B@4	mt	H-mt1.15	154.2	15.2329	0.0005	0.346330	0.000036	0.00018369	0.00000042	no	15.2336	0.3463	-0.51	0.13	-0.86	0.30
LP-B@5	mt	H-mt1.21	173.4	15.2332	0.0006	0.346318	0.000043	0.00018439	0.00000035	no	15.2339	0.3463	-0.49	0.13	-0.89	0.30
LP-B@6	mt	H-mt1.22	171.5	15.2350	0.0006	0.346533	0.000033	0.00018346	0.00000035	no	15.2357	0.3465	-0.37	0.13	-0.28	0.29
LP-B@7	mt	H-mt1.30	100.9	15.2343	0.0007	0.346384	0.000030	0.00018187	0.00000035	no	15.2350	0.3464	-0.42	0.13	-0.71	0.29
LP-B@8	mt	H-mt1.31	106.3	15.2368	0.0006	0.346437	0.000041	0.00018302	0.00000035	no	15.2375	0.3465	-0.25	0.13	-0.55	0.30
LP-D@1	mt	H-mt1.2	177.7	15.2335	0.0005	0.346560	0.000044	0.00016590	0.00000034	no	15.2342	0.3466	-0.47	0.13	-0.20	0.31
LP-D@10	mt	H-mt1.39	140.9	15.2357	0.0004	0.346420	0.000036	0.00016579	0.00000032	no	15.2364	0.3464	-0.32	0.13	-0.61	0.30
LP-D@11	mt	H-mt1.40	130.1	15.2350	0.0005	0.346494	0.000023	0.00016560	0.00000032	no	15.2356	0.3465	-0.37	0.13	-0.39	0.29
LP-D@12	mt	H-mt1.45	134.3	15.2371	0.0008	0.346530	0.000041	0.00016585	0.00000032	no	15.2378	0.3465	-0.23	0.13	-0.29	0.30
LP-D@13	mt	H-mt1.46	133.8	15.2352	0.0006	0.346353	0.000029	0.00016582	0.00000034	no	15.2359	0.3464	-0.36	0.13	-0.80	0.29
LP-D@14	mt	H-mt1.47	124.0	15.2367	0.0005	0.346467	0.000023	0.00016643	0.00000032	no	15.2374	0.3465	-0.26	0.13	-0.47	0.29
LP-D@15	mt	H-mt1.52	130.2	15.2326	0.0006	0.346322	0.000020	0.00016615	0.00000032	no	15.2333	0.3463	-0.53	0.13	-0.89	0.28
LP-D@16	mt	H-mt1.57	156.0	15.2349	0.0004	0.346387	0.000033	0.00016592	0.00000034	no	15.2356	0.3464	-0.38	0.13	-0.70	0.29
LP-D@17	mt	H-mt1.58	144.7	15.2316	0.0005	0.346182	0.000038	0.00016659	0.00000031	no	15.2322	0.3462	-0.60	0.13	-1.29	0.30
LP-D@2	mt	H-mt1.3	186.2	15.2361	0.0005	0.346534	0.000040	0.00016683	0.00000034	no	15.2368	0.3465	-0.30	0.13	-0.28	0.30
LP-D@3	mt	H-mt1.9	174.4	15.2342	0.0007	0.346406	0.000029	0.00016641	0.00000033	no	15.2349	0.3464	-0.42	0.13	-0.65	0.29
LP-D@4	mt	H-mt1.10	188.1	15.2330	0.0006	0.346461	0.000043	0.00016700	0.00000033	no	15.2336	0.3465	-0.50	0.13	-0.49	0.30
LP-D@5	mt	H-mt1.16	171.2	15.2326	0.0007	0.346503	0.000040	0.00016643	0.00000035	no	15.2333	0.3465	-0.53	0.13	-0.37	0.30
LP-D@6	mt	H-mt1.17	189.8	15.2409	0.0009	0.346944	0.000037	0.00016237	0.00000033	no	15.2416	0.3470	0.02	0.14	0.91	0.30
LP-D@7	mt	H-mt1.23	163.7	15.2376	0.0006	0.346470	0.000032	0.00016221	0.00000037	no	15.2382	0.3465	-0.20	0.13	-0.46	0.29
LP-D@8	mt	H-mt1.24	174.3	15.2375	0.0004	0.346473	0.000027	0.00016497	0.00000034	no	15.2382	0.3465	-0.20	0.13	-0.45	0.29
LP-D@9	mt	H-mt1.32	92.0	15.2355	0.0005	0.346515	0.000036	0.00016616	0.00000037	no	15.2362	0.3465	-0.34	0.13	-0.33	0.30
LP-E@1	mt	H-mt1.6	161.9	15.2285	0.0004	0.346287	0.000031	0.00015038	0.00000032	no	15.2291	0.3463	-0.80	0.13	-0.99	0.29
LP-E@2	mt	H-mt1.13	153.6	15.2311	0.0007	0.346629	0.000049	0.00015065	0.00000032	no	15.2317	0.3466	-0.63	0.13	-0.01	0.31
LP-E@3	mt	H-mt1.20	161.9	15.2326	0.0006	0.346411	0.000037	0.00015180	0.00000031	no	15.2332	0.3464	-0.53	0.13	-0.64	0.30
LP-E@4	mt	H-mt1.29	120.4	15.2300	0.0009	0.346210	0.000032	0.00014021	0.00000030	no	15.2305	0.3462	-0.71	0.14	-1.22	0.29
LP-E@5	mt	H-mt1.35	140.9	15.2302	0.0008	0.346248	0.000028	0.00015076	0.00000032	no	15.2308	0.3463	-0.69	0.13	-1.11	0.29
LP-E@6	mt	H-mt1.36	139.6	15.2303	0.0006	0.346334	0.000040	0.00015183	0.00000031	no	15.2309	0.3463	-0.68	0.13	-0.86	0.30
LP-E@7	mt	H-mt1.41	115.5	15.2307	0.0009	0.346170	0.000036	0.00015138	0.00000036	no	15.2313	0.3462	-0.66	0.14	-1.33	0.30
LP-E@8	mt	H-mt1.42	133.8	15.2305	0.0008	0.346258	0.000029	0.00015069	0.00000035	no	15.2311	0.3463	-0.67	0.13	-1.08	0.29
El Laco magnetite (reference: δ^{56}Fe = 0.261 ‰)																
EL-2@1	mt	H-mt1.25	142.8	15.2463	0.0005	0.346891	0.000031			no	15.2463	0.3469	0.32	0.13	0.71	0.29
EL-2@2	mt	H-mt1.26	124.0	15.2471	0.0006	0.346864	0.000033			no	15.2471	0.3469	0.38	0.13	0.63	0.29
EL-2@3	mt	H-mt1.33	143.3	15.2464	0.0006	0.346828	0.000029			no	15.2464	0.3468	0.33	0.13	0.53	0.29

continued next page

Table DR3 continued

Filename	Mineral	Session.run[a]	^{56}Fe cps x 10^6	$^{56}Fe/^{54}Fe$ raw	±σ	$^{57}Fe/^{54}Fe$ raw	±σ	$^{53}Cr/^{54}Fe$ raw[b]	±σ	Drift corr.[c]	$^{56}Fe/^{54}Fe$ corr.[d]	$^{57}Fe/^{54}Fe$ corr.[d]	$\delta^{56}Fe$[e] (‰)	±σ	$\delta^{57}Fe$[e] (‰)	±σ
EL-2@4	mt	H-mt1.34	0.0	15.2438	0.0004	0.346765	0.000032			no	15.2438	0.3468	0.16	0.13	0.35	0.29
EL-2@5	mt	H-mt1.37	142.3	15.2460	0.0006	0.346877	0.000032			no	15.2460	0.3469	0.31	0.13	0.67	0.29
EL-2@6	mt	H-mt1.38	141.5	15.2493	0.0006	0.346841	0.000022			no	15.2493	0.3468	0.53	0.13	0.57	0.29
EL-2@7	mt	H-mt1.43	128.1	15.2497	0.0005	0.346856	0.000031			no	15.2497	0.3469	0.55	0.13	0.61	0.29
EL-2@8	mt	H-mt1.44	117.7	15.2512	0.0006	0.346970	0.000034			no	15.2512	0.3470	0.65	0.13	0.94	0.30
EL-3@1	mt	H-mt1.48	124.6	15.2450	0.0005	0.346595	0.000033			no	15.2450	0.3466	0.24	0.13	-0.14	0.29
EL-3@2	mt	H-mt1.49	128.6	15.2413	0.0006	0.346718	0.000043			no	15.2413	0.3467	0.00	0.13	0.21	0.30
EL-3@3	mt	H-mt1.50	128.3	15.2385	0.0006	0.346534	0.000035			no	15.2385	0.3465	-0.19	0.13	-0.32	0.30
EL-3@4	mt	H-mt1.51	127.0	15.2420	0.0006	0.346679	0.000035			no	15.2420	0.3467	0.05	0.13	0.10	0.30
EL-3@5	mt	H-mt1.53	0.0	15.2396	0.0005	0.346554	0.000030			no	15.2396	0.3466	-0.11	0.13	-0.26	0.29
EL-3@6	mt	H-mt1.54	153.6	15.2411	0.0008	0.346550	0.000030			no	15.2411	0.3466	-0.02	0.13	-0.27	0.29
EL-3@7	mt	H-mt1.55	153.8	15.2402	0.0006	0.346629	0.000040			no	15.2402	0.3466	-0.08	0.13	-0.05	0.30
EL-3@8	mt	H-mt1.56	154.5	15.2436	0.0006	0.346719	0.000030			no	15.2436	0.3467	0.15	0.13	0.21	0.29
EL-4@1	mt	H-mt1.59	141.4	15.2531	0.0007	0.346988	0.000031			no	15.2531	0.3470	0.77	0.13	0.99	0.29
EL-4@2	mt	H-mt1.60	140.4	15.2521	0.0007	0.346911	0.000025			no	15.2521	0.3469	0.71	0.13	0.77	0.29
EL-4@3	mt	H-mt1.61	143.3	15.2530	0.0007	0.346970	0.000028			no	15.2530	0.3470	0.77	0.13	0.94	0.29
EL-4@4	mt	H-mt1.62	133.4	15.2586	0.0009	0.347166	0.000031			no	15.2586	0.3472	1.14	0.14	1.50	0.29
Balmat pyrite (reference: $\delta^{56}Fe$ = -0.399 ‰)																
Bal_A2-x1	py	H-py1.1	83.3	15.1689	0.0008	0.344462	0.000049			no	15.1689	0.344462	-0.55	0.23	-0.55	0.30
Bal_A2-x2	py	H-py1.3	82.6	15.1725	0.0006	0.344607	0.000059			no	15.1725	0.344607	-0.30	0.23	-0.13	0.31
Bal_A2-x3	py	H-py1.5	83.7	15.1756	0.0007	0.344393	0.000052			no	15.1756	0.344393	-0.10	0.23	-0.75	0.30
Bal_A2-x4	py	H-py1.7	84.9	15.1716	0.0006	0.344401	0.000045			no	15.1716	0.344401	-0.37	0.23	-0.73	0.29
Bal_A2-x5	py	H-py1.9	86.0	15.1668	0.0007	0.344400	0.000059			no	15.1668	0.344400	-0.68	0.23	-0.73	0.31
Bal_C-x1	py	H-py1.2	81.9	15.1758	0.0010	0.344683	0.000043			no	15.1758	0.344683	-0.09	0.23	0.09	0.29
Bal_C-x2	py	H-py1.4	82.3	15.1725	0.0008	0.344688	0.000057			no	15.1725	0.344688	-0.30	0.23	0.11	0.31
Bal_C-x3	py	H-py1.6	83.5	15.1753	0.0008	0.344526	0.000050			no	15.1753	0.344526	-0.12	0.23	-0.36	0.30
Bal_C-x4	py	H-py1.8	84.3	15.1740	0.0008	0.344522	0.000066			no	15.1740	0.344522	-0.20	0.23	-0.38	0.32
Fe_pos_test_A	py	H-py2.1	230.2	15.1773	0.0004	0.344376	0.000020			no	15.1773	0.344376	-0.38	0.04	-0.65	0.10
Fe_pos_test_A@1	py	H-py2.3	231.6	15.1770	0.0004	0.344381	0.000020			no	15.1770	0.344381	-0.40	0.04	-0.63	0.10
Fe_pos_test_A@2	py	H-py2.7	236.4	15.1775	0.0004	0.344440	0.000017			no	15.1775	0.344440	-0.37	0.04	-0.46	0.10
Fe_pos_test_A@3	py	H-py2.8	237.1	15.1765	0.0004	0.344405	0.000019			no	15.1765	0.344405	-0.44	0.04	-0.56	0.10
Fe_pos_test_B	py	H-py2.4	228.5	15.1777	0.0003	0.344507	0.000016			no	15.1777	0.344507	-0.36	0.04	-0.27	0.10
Fe_pos_test_B@1	py	H-py2.5	229.6	15.1744	0.0006	0.344433	0.000020			no	15.1744	0.344433	-0.57	0.05	-0.48	0.10
Fe_pos_test_B@2	py	H-py2.6	230.8	15.1744	0.0004	0.344293	0.000023			no	15.1744	0.344293	-0.57	0.04	-0.89	0.11
Fe_pos_test_C	py	H-py2.9	232.2	15.1812	0.0004	0.344540	0.000025			no	15.1812	0.344540	-0.12	0.04	-0.17	0.11
Fe_pos_test_C@1	py	H-py2.2	236.4	15.1785	0.0004	0.344539	0.000016			no	15.1785	0.344539	-0.30	0.04	-0.17	0.10

[a] Refers to analytical session and sequence number in that session (i.e. H-mt1.6 = homogeneity trial, magnetite session1, run number 6)

[b] Omitted where ^{53}Cr count rate is sufficiently low that correction results in <0.01 ‰ correction on $\delta^{56}Fe$.

[c] Indicates whether raw data have been corrected for linear drift within the session and, if so, the magnitude of drift (in ‰/run) for $^{56}Fe/^{54}Fe$ and $^{57}Fe/^{54}Fe$ respectively.

[d] Raw corrected for possible within session drift and interference from ^{54}Cr on ^{54}Fe.

[e] Assumes $\delta^{56}Fe$ = -0.375 ‰ and $\delta^{57}Fe$ = -0.542 ‰ for the LP-204 magnetite grain LP-D; $\delta^{56}Fe$ = -0.399 ‰ and $\delta^{57}Fe$ -0.577 ‰ for Balmat pyrite grain A.